Journal of Intelligent Material Systems and Structures
http://jim.sagepub.com/

Linear magnetorheological brake with serpentine flux path as a high force and low off-state friction actuator for haptics

Mustafa S Alkan, Hakan Gurocak and Berk Gonenc

Journal of Intelligent Material Systems and Structures 2013 24: 1699 originally published online 5 April 2013
DOI: 10.1177/1045389X13484098

Original Article

Journal of Intelligent Material Systems and Structures

Journal of Intelligent Material Systems and Structures
24(14) 1699–1713

DOI: 10.1177/1045389X13484098
jim.sagepub.com
SAGE

Linear magnetorheological brake with serpentine flux path as a high force and low off-state friction actuator for haptics

Mustafa S Alkan, Hakan Gurocak and Berk Gonenc

Abstract
In robotics and haptics, actuators that are capable of high force output with compact size are desired for stable and stiff interfaces. Magnetorheological brakes are viable options for such implementations since they have large force-to-volume ratios. Existing linear magnetorheological brakes have limited strokes, are relatively large, and have high off-state friction forces mainly due to the piston-cylinder internal design. The main contribution of this research is a new alternative internal design for linear magnetorheological brakes. The proposed approach uses the serpentine flux path concept to eliminate the piston-cylinder arrangement. It leads to significantly less off-state friction and infinite stroke. To the best of our knowledge, this is the first such linear magnetorheological brake. Our new brake can produce 173-N force. In comparison, a conventional linear magnetorheological brake with the same size can only produce about 27-N force. Our results showed that the ratio of the off-state friction force to the maximum force output in the prototype linear brake is about 3% compared with more than 10% for most similar devices in the literature and 27% for a commercial brake. At the same time, the compactness was improved as our prototype is about half the size of a commercially available product.

Keywords
Linear magnetorheological brake, magnetorheological damper, magnetorheological fluid, haptics, serpentine flux path, off-state friction

Introduction

During the past few decades, the popularity of magnetorheological (MR) fluids in the industry has been increasing dramatically. MR brakes are actuators that use this smart fluid to create braking torque or force by controlling its viscosity. The fluid is normally similar to low-viscosity oil, but it becomes a thick medium upon exposure to magnetic flux. MR brakes are quite popular in many applications, including prosthetics, automotive, vibration stabilization, and haptics, owing to the desirable characteristics, such as high force-to-volume ratio, inherent stability, and simple interface between the mechanical and the electrical systems.

Increasing the force output of the brake can be achieved by increasing either the size of the brake or the input current. The increased size is undesirable for many applications such as haptics and automation. Increased current causes problems in terms of safety and heating, limiting the usage. The linear MR brakes currently available on the market and in the literature are able to produce large forces, but the piston-cylinder arrangement in the brake design amplifies the friction force at the fluid gap to a large pressure difference between the faces of the piston. This leads to a significant off-state force, which is uncontrollable and which is what the actuator applies even when the input current is turned off. Such a force is undesirable in many applications, especially in haptics. Haptic interfaces implementing such actuators keep applying forces on the user's hand even when the user is not interacting with objects in a virtual simulation environment, hence reducing the realism of the interaction.

The main contribution of this research is a new alternative internal design for linear MR brakes. The

School of Engineering and Computer Science, Washington State University, Vancouver, WA, USA

Corresponding author:
Hakan Gurocak, School of Engineering and Computer Science, Washington State University, 14204 NE Salmon Creek Ave., Vancouver, WA 98686, USA.
Email: hgurocak@vancouver.wsu.edu

proposed approach uses the *serpentine flux path* concept to eliminate the conventional piston-cylinder arrangement. It leads to significantly less off-state friction and facilitates devices with infinite stroke. To the best of our knowledge, this is the first such linear MR brake. Our research group first introduced the serpentine flux path concept for *rotary* MR brakes (Blake and Gurocak, 2009). Recently, we also developed an optimization method for such rotary MR brakes (Erol and Gurocak, 2011). This approach enables activation of the whole MR fluid on the contact surface with a smaller magnetomotive force by weaving the magnetic flux through the MR fluid multiple times. For example, using this technique, an actuator with 33% smaller diameter yet 2.7 times more torque capability than a commercial brake was manufactured (Senkal and Gurocak, 2010).

The MR brakes provide quick response with simple control. When used alone or in combination with active actuators, MR brakes have been proven to provide realistic rigid virtual object simulations in haptic applications (An and Kwon, 2002, 2008; Nam and Park, 2007; Reed and Book, 2004). There is a commercial linear MR brake (model RD-1005) by Lord Corporation, which was tested several times to model the response of the mechanical equipment (Dominguez et al., 2006; Li et al., 2000; Xiang et al., 2008). This brake has about 3.8-cm diameter, 208.3-mm extended length, and was experimented to provide 451-N force at 1.5-A current input and 0.2-m/s velocity. However, the off-state friction was measured to be 52 N for the same speed with no magnetic field. Another commercial product from Lord Corporation (Rheonetics SD-1000-2) was also assessed (Li et al., 1998). The linear MR brake has a diameter of 1.75 in and a nominal length of 4 in. The force at 1.5 A of current and 0.2 m/s of velocity is shown to be 2.1 kN, while the off-state friction force at this speed was noted as 270 N. A linear MR brake was constructed to implement into prosthetics (Li et al., 2006). The brake had a diameter of 30 mm and a length of 130 mm. The braking force when activated was shown as 942 N, while the off-state force was shown as 94 N. An MR brake was optimally designed and manufactured (Gavin et al., 2001). The diameter of the cylinder was given as 46.228 mm. The device was capable of 4 kN of force when activated to 10 A of current and 0.3 kN of force when deactivated. Another study focused on the investigation and control of linear MR brakes (Milecki, 2000). The diameter of the brake was given as 50 mm. The brake was capable of exerting 12 kN of force when the coil was activated with 1.4 A of current at the speed of 50 mm/s. The off-state force at the same speed was shown to be 4 kN. In general, most linear MR dampers in the literature have an off-state force that is more than 10% of their fully activated force.

Our new linear MR brake has infinite stroke. If larger stroke is required for an application, a longer cylinder is needed. This means a bigger actuator. Therefore, a bulkier actuator delivers the same amount of force just because a larger stroke is needed. With our design, the same compact brake body can be used for any stroke requirement without size modification in the actuator body. This provides a wide application area and great flexibility in haptic interface design. Furthermore, our new linear brake has a minimized off-state friction force of 5.4 N. This is about 3% of the 170 N fully activated force of the device. The size of the brake was reduced with the serpentine magnetic flux path methodology. Further reduction in the off-state force was obtained by applying a reverse current pulse to remove the residual magnetic field in the brake.

In the following sections, we will first present the details of the new MR brake design. This will be followed by details of experiments to quantify the performance of the brake prototype by several experiments, namely, virtual wall collision, damping, Coulomb friction simulations for haptics, and performance with varying input currents. The article concludes with the discussion of the results.

Linear MR brake with serpentine flux path

Off-state force in typical linear MR brakes

The existing linear MR brake designs are similar to an ordinary shock absorber. In these designs, the fluid chamber in a shock absorber is filled with MR fluid instead of viscous oil and the piston is modified to generate a magnetic field by means of a built-in coil (Figure 1). Even though the volume of activated fluid is not large in these designs, they are capable of giving large forces due to the big pressure difference between the two faces of the piston. However, this design leads to significant off-state friction force as the small amount of shear stress due to plastic viscosity at the MR fluid is amplified to a high-pressure difference across the piston.

In these designs, the total pressure difference across the piston can be computed using the following formula (Gavin et al., 2001)

$$\Delta P_{tot} \approx 2.1 \frac{\tau_{yd}}{g} + \Delta P_{off} \tag{1}$$

where τ_{yd} is the MR fluid yield stress, "g" is the fluid gap thickness, and the ΔP_{off} term corresponds to the pressure difference across the piston due to the uncontrollable off-state friction. It is given by

$$\Delta P_{off} \approx \frac{12Q\eta(2L_p)}{\pi(D_p + g)g^3} \tag{2}$$

where "Q" is the volumetric flow rate, "η" is the plastic viscosity of the fluid at the corresponding speed, L_p is

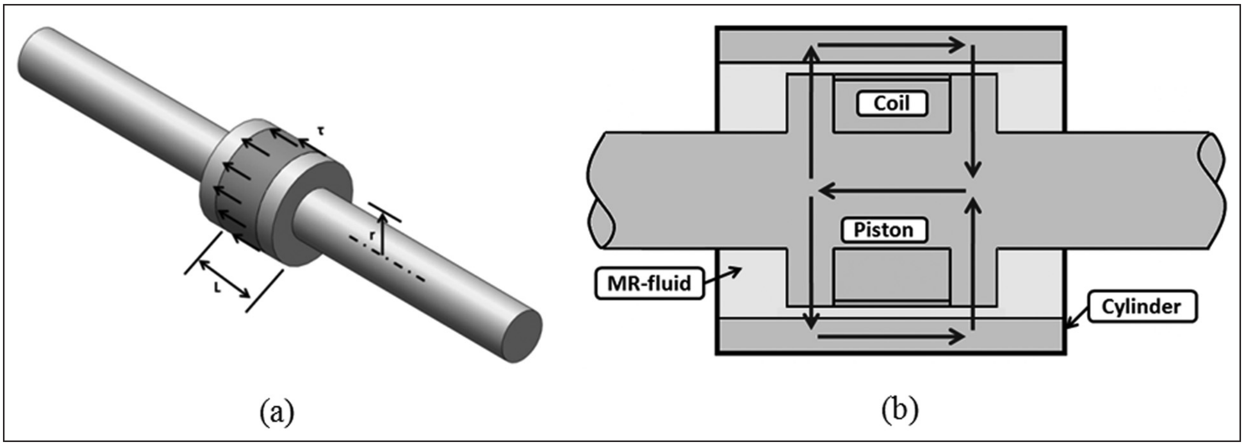

Figure 1. (a) Three-dimensional view of the piston. (b) The magnetic flux path shown on the sectional view of the linear MR brake assembly available on the market.
MR: magnetorheological.

Table 1. Parameters used in the estimate off-state force calculation of a linear magnetorheological (MR) brake in the literature (Li et al., 2006).

Parameter	Value
Inner diameter of the cylinder (mm)	23.5
Outer diameter of the piston (mm)	23
Diameter of the rod (mm)	9
Pole length (mm)	5
Pole gap (mm)	0.3
Speed of the rod (mm/s)	30
Plastic viscosity (Pa s)[a]	0.3

[a]Estimated from a commercial MR fluid (Lord MRF-140 CG).

the piston length (excluding the coil), and D_p is the piston diameter. The total force can then be computed by multiplying the pressure difference with the area that the pressure is applied

$$F = \Delta P_{tot} \cdot \left(\pi \frac{D_p^2 - D_r^2}{4} \right) \tag{3}$$

where D_r is the diameter of the rod. In addition to this force, there are additional forces due to bushings and seals in practical applications.

To illustrate the drawback of the existing designs in terms of off-state force contribution, a designed MR brake in the literature (Li et al., 2006) is analyzed using the formulas shown in equations (2) and (3). The geometric parameters of the MR brake and the constants estimated during the computation are shown in Table 1. The off-state force is estimated by neglecting the contribution of the on-state (zero on-state shear stress τ_{yd}). Using the mentioned formulas, the computed off-state force due to the pressure difference across the piston is 71 N. This calculation is only performed for 30 mm/s rod speed. If it was considered 10 times more as in our case (300 mm/s), the off-state force contribution might have also been increased 10 times more (712 N).

New linear brake without a piston

MR fluids are commonly modeled using either Herschel–Bulkley or Bingham plastic models. The main difference between these models is in how they account for the contribution of the shear rate to the resulting shear stress. Here, the Bingham plastic model was selected due to its simplicity. The governing equation for this model is

$$\tau = \tau_{yd}(B) + \eta\gamma \tag{4}$$

where τ_{yd} is the dynamic yield stress, depending on the magnetic flux. The second term in this equation is the shear stress related to the motion, where η is the plastic viscosity and γ is the shear rate. Significant part of the force consists of the dynamic yield stress acting on the contact surface covered by the MR fluid. This corresponds to the first term in equation (4). The second term in the equation is the uncontrollable shear stress contribution, which is the source of the friction force when the device is turned off (off-state). The shear rate depends on the relative speed of the two moving surfaces and the thickness of the MR fluid gap between the surfaces ($\gamma = velocity/fluid\,gap$).

In haptic applications, it is desirable to have low off-state forces. Hence, the viscous forces in the linear brake need to be minimized. To achieve this, we removed the piston and instead used a constant diameter rod (Figure 3). This has the advantage of eliminating the viscous force that would otherwise be applied on the piston due to the pressure difference across it.

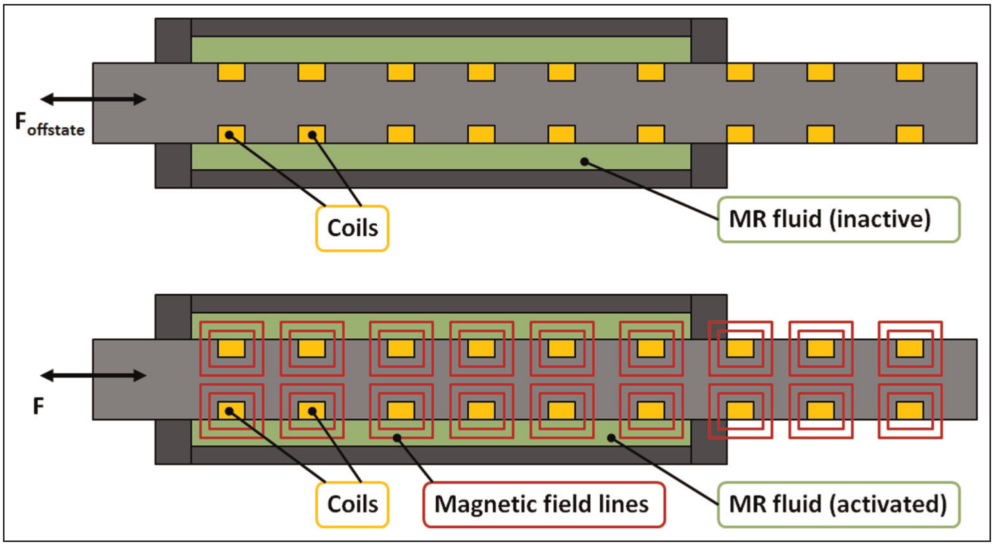

Figure 2. Alternative conceptual design option.

For preliminary design considerations, the off-state viscous friction force was estimated with respect to the worst case considering the maximum speed that the rod could attain. The largest speed requirement was considered as 300 mm/s. Then, the shear rate for this speed was found from $\gamma = velocity\,(300\,\text{mm/s})/fluid\ gap$ (0.01 in) as 1184 s^{-1}. The fluid shear stress for this shear rate was given as 230 Pa in the datasheet supplied from the manufacturer (BASF Corp). Then, the force over the contact area was computed as 0.43 N. On the contrary, when the brake is turned on, the shear stress of the fluid is given as 106 kPa in the datasheet, which corresponds to 170 N of force over the contact area. Therefore, the off-state viscous friction force due to the plastic viscosity of the MR fluid in the second term of equation (4) can be neglected compared with the on-state. Hence, including the Coulomb friction from the seals and bushings, the total braking force can be written as

$$F = 2\pi \cdot r \cdot L \cdot \tau_{yd}(B) + F_{Coulomb} \tag{5}$$

where $\tau_{yd}\,(B)$ is the MR fluid yield stress as a function of magnetic flux B, r is the radius of the rod, L is the length of the active area of the rod, and $F_{Coulomb}$ is the mechanical friction force (mainly from seals and bushings).

Serpentine flux path. The existing linear MR brakes employ a coil embedded in the piston. In such a design, the magnetic flux goes through a large cross-sectional area reducing the resulting flux density. To increase the magnetic flux density and the force output of the brake, one approach is to increase the rod radius, coil windings, and current. All of these lead to bulkier designs with high inertia. Another option is to make the piston and rod diameters the same and use several coils on the rod as shown in Figure 2.

This design has the advantage of eliminating the flow mode since it only employs shear mode. However, it comes with many disadvantages. Addition of multiple coils will increase the inertia and the size of the actuator. Since the coils will be moving in and out of the actuator casing, sealing the fluid in the actuator will be problematic. The increased number of coils and their wires will create a cable management issue that becomes a design, fabrication, and maintenance challenge. Also, the actuator stroke will be limited, since if the rod is pulled out of the casing too far, some of the coils will be outside the fluid resulting in a drop in the force output.

In our design, we employed magnetically nonconductive aluminum sections and magnetically conductive steel (1018 steel) materials and two coils positioned horizontally above and below the rod. The geometric configuration of the conductive and nonconductive materials was strategically arranged to bend the magnetic field and weave it through the MR fluid gap multiple times to expose more of the fluid to the flux (Figure 3(a)). Therefore, the resulting brake is more compact and the braking force is increased without increasing the size of the coils or the rod.

MagNet, a finite element analysis (FEA) software by Infolytica Corp., was used to model the brake to verify the design before manufacturing. The design optimization was based on the magnetic flux density result for the MR fluid in the gap. The size of various parts in the design was altered to maximize the flux density in the fluid, leading to increased braking force, while keeping the overall size compact. The maximum force requirement was set at 170 N initially. The magnetic coil was formed with 250 turns of 28-gauge enameled magnet wire on both upper and lower sides of the

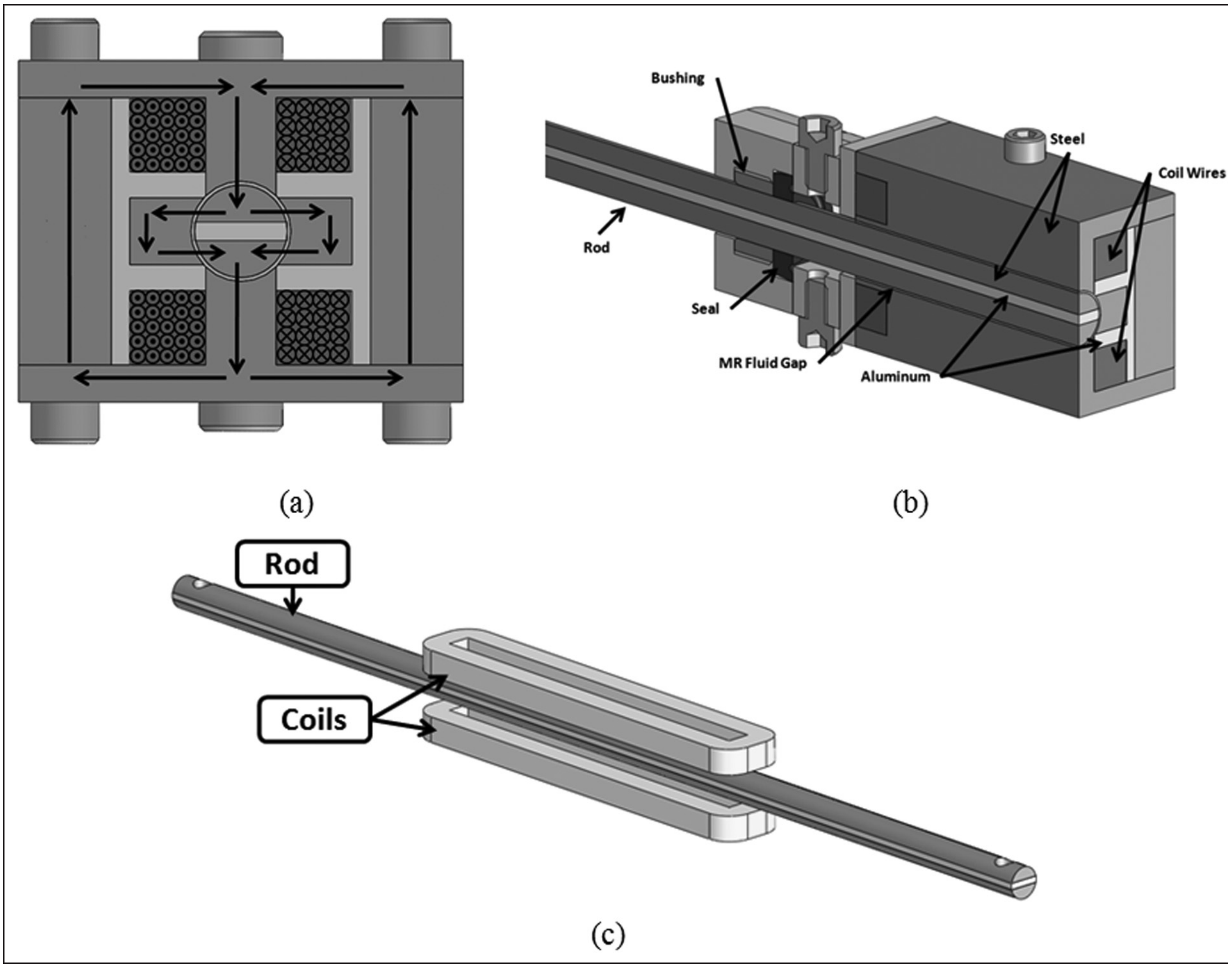

Figure 3. (a) Serpentine magnetic flux path weaving through the rod and the case. It enables activation of more of the magnetorheological (MR) fluid to provide more force. (b) Assembly showing the MR fluid in the gap activated by the coils on the upper and lower sides. (c) Coil placements on the upper and lower sides of the rod.
MR: magnetorheological.

rod. The MR fluid (Basonetic 5030) was from BASF. The rod has two half cylinders made of steel and a thin layer of aluminum plate in between. This specific geometry helped us weave the magnetic flux path by keeping the coil size four times less than the one in the case of only one pass of the flux path over the entire rod. The magnet wire was wound around the upper side and lower side of the rod (Figure 3(c)), which was also made of steel to conduct the magnetic field generated by the coil. The assembly of the actuator is shown in Figure 3(b).

The shear stress on the MR fluid is directly proportional to the magnetic flux generated by the coil, which depends on both the current passing through the magnet wires and the number of turns in the coil. The flux increases with the increase in the number of turns and the amount of current. Both of these might limit the compactness requirement set initially. Since the thickness of the wire needs to be increased for larger currents to pass, the total size of the coil will get larger while keeping the number of turns the same as before. Another option might be using more turns by using a thinner wire for the same range of current. However, this results in overheating of the wires since the total length is increased and the cross-sectional area is reduced.

Fluid gap is another important parameter that determines the braking force. As the gap gets smaller, the magnetic flux in the gap becomes larger since the magnetic permeability of the MR fluid is quite smaller than the low-carbon steel. The magnetic circuit equivalent of the brake can be presented with the following equation

$$F = \Phi \cdot R \tag{6}$$

where "F" is the magnetomotive force, "Φ" is the magnetic flux, and "R" is the equivalent reluctance of the magnetic circuit loop. The reluctance of each material in the loop can be computed using the following formula:

$$R = \frac{l}{A \cdot \mu} \tag{7}$$

Parameter	Value
R_1	3.175 mm
L_1	1.854 mm
L_2	6.350 mm
L_3	5.130 mm
L_4	4.064 mm
θ_1	7.6°
θ_2	33.7°
Number of coil turns (for one side)	250 turns
Max. force output	170 N (theoretical) 173.3 N (experimental)
Max. current	1 A

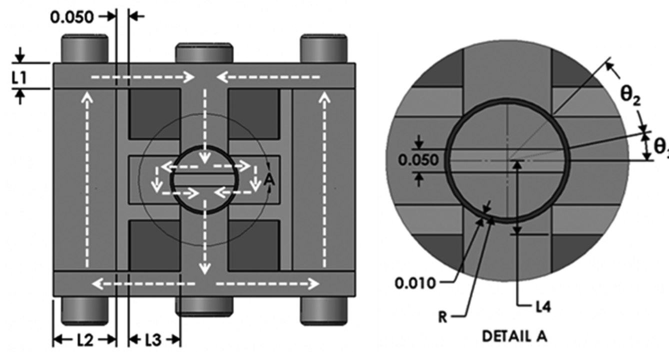

Figure 4. Design parameters of the new linear MR brake.
MR: magnetorheological.

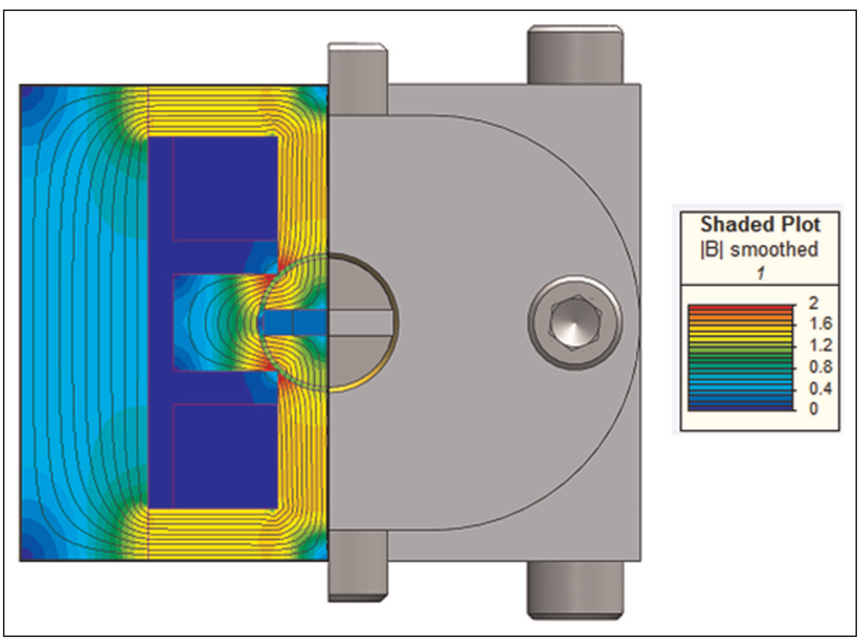

Figure 5. FEA results showing the serpentine flux path inside the MR brake. The MR fluid in the contact surface is magnetically activated to 1.2 T when the input current is set to 1 A.
FEA: Finite element analysis; MR: magnetorheological.

where "l" is the longitudinal distance (which is the fluid gap for MR fluid), "A" is the sectional area perpendicular to the magnetic flux direction, and "μ" is the magnetic permeability of the material. As seen from the equations, increased fluid gap increases the magnetic reluctance of the MR fluid in equation (7), which leads to a smaller magnetic flux (Φ) in equation (6), provided the magnetomotive force "F" is kept constant.

The values of our final design parameters are presented in Figure 4. Accordingly, the rod diameter was set to 6.35 mm, which is a standard round stock size. To get the desired force (170 N), the length was kept as 86.36 mm. The fluid gap (radial clearance) was left as 0.254 mm, which resulted in 1.2 T flux on the MR fluid (Figure 5). The shear stress in saturation corresponding to this flux rate was given as 106 kPa in the

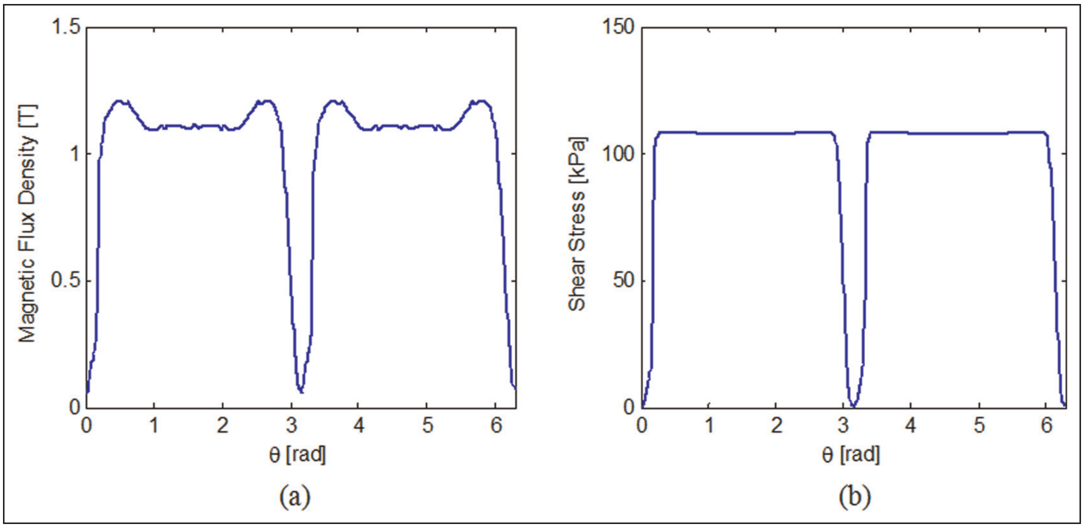

Figure 6. FEA results showing the distribution of magnetic flux density: (a) magnetic flux density over the MR fluid around the rod. Angular position θ starts from the horizontal axis and increases in the counter clockwise direction. (b) Shear stress generated by the MR fluid as a function of θ.
FEA: Finite element analysis; MR: magnetorheological.

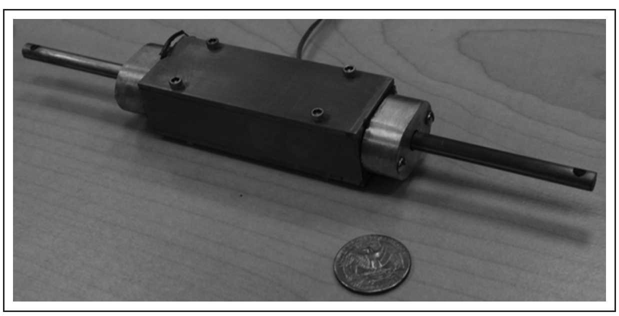

Figure 7. Manufactured prototype MR brake.
MR: magnetorheological.

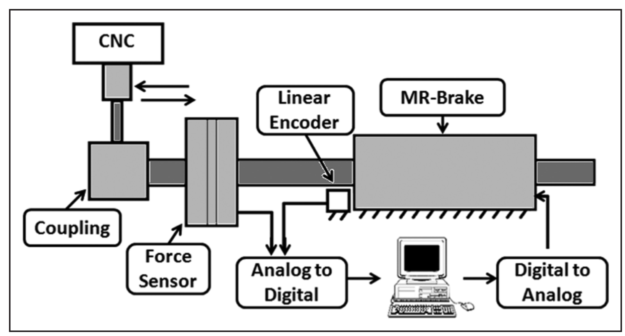

Figure 8. Experimental setup.
MR: magnetorheological.

manufacturer's datasheet. The force was then calculated using the area of the steel sections on the rod, and this shear stress based on equation (5). The activated fluid surface area is 0.0016 m^2. Therefore, the force is about 170 N. After building a prototype actuator, we experimentally found the maximum force to be 173.3 N at 1-A current and the Coulomb friction due to the seals as 5.4 N (experimental details are explained in section "Experiments and results"). The magnetic flux density over the MR fluid and the corresponding shear stress distribution are shown in Figure 6.

Experiments and results

We manufactured a prototype linear MR brake to assess its performance experimentally. The manufactured prototype is shown in Figure 7. The setup included a force transducer from ATI Industrial Automation (mini45-E), which was mounted at the end of the rod, and a high-resolution linear encoder measuring the position of the brake rod. For data acquisition, Quanser Q4 Series hardware coupled with MATLAB/SIMULINK via WinCon software was employed. The instrumented brake was mounted on the table of a computer numerical control (CNC) mill to provide accurately controlled input forces (Figure 8).

Braking force

In this experiment, the goal was to determine the braking force at various levels of current passing through the coils. While the current was incremented from 0 to 1 A with increments of 0.1 A, the force on the sensor was recorded. The change in the force with respect to current is presented in Figure 9. The minimum force when the current is off and the maximum force at 1 A of current were noted, respectively, as 5.4 and 173.3 N, respectively. This results in a dynamic range of around

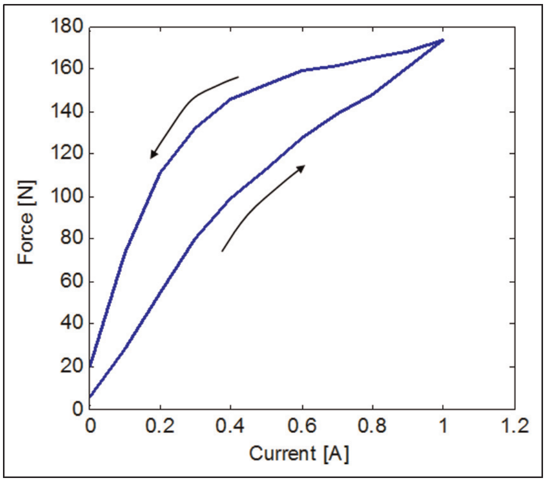

Figure 9. Braking force as a function of input current. The current is first increased and then decreased, showing some hysteresis behavior.

30.1 dB and 167.9 N controllable force (= 173.3 − 5.4). The controllable range was computed using FEA analysis as 170 N. The small difference can be due to the manufacturing inaccuracies.

Wall collision

The prototype brake was used as a 1-degree-of-freedom (DOF) haptic device. In this experiment, it was aimed to quantify how well the brake could simulate a collision with a virtual wall (plane). The experimental setup is presented in Figure 10. The data acquisition system was set to run at 1000 Hz. The current given to the coils was set to high (1 A) when collision occurred. Two different strategies were followed to carry out this experiment.

In the first case, the force sensor was not used. The brake was activated when the end-effector contacted and slightly penetrated into the virtual wall and deactivated when it was outside the wall. The control logic for this case is shown in Figure 12(a). Results of virtual wall simulation without the force sensor are given in Figure 11.

In the second case, the force sensor was used to detect the direction of the force applied by the user (Figure 12(b)). The control loop also included demagnetizing, giving a reverse current for a short period to eliminate hysteresis in the brake. The duration for demagnetization was tuned to 0.05 s. The brake seemed to have no extra force due to hysteresis after applying this to the control system. Figure 13 shows the results of virtual wall simulation with the force sensor.

Damping experiment

This experiment quantified how well the MR brake could represent a virtual damper. Variable levels of current were supplied to the brake through a servo amplifier and data acquisition board. For such a system, the desired force can be computed as

$$F = b \cdot v \tag{8}$$

where "b" denotes the simulated damping ratio and "v" is the rod velocity. The results of the damping experiment for two sample cases with low and high damping ratios (100 N s/m on the left and 700 N s/m on the right) are presented in Figure 14.

Coulomb friction experiment

This experiment explored how the MR brake can simulate Coulomb friction in a haptic application, as Karnopp model was employed in our experiment (An and Kwon, 2006). The model uses a velocity threshold value to define static friction range instead of using absolute zero velocity since it is very difficult to obtain absolute zero velocity with the digital encoder systems due to discretization. The model is represented as

$$F_{friction} = \begin{cases} F_{dynamic} \cdot \mathrm{sgn}(v) & |v| > v_{thresold} \\ \max(F_{static}, F_{applied}) & |v| < v_{threshold} \end{cases} \tag{9}$$

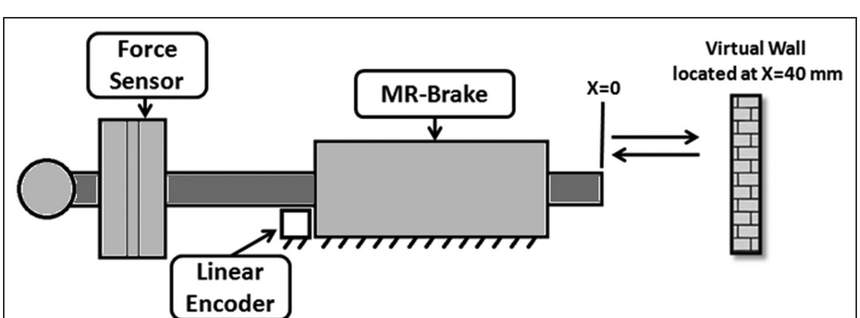

Figure 10. Virtual wall collision experimental setup. The user collides with the virtual wall located at position x = 40 mm.
MR: magnetorheological.

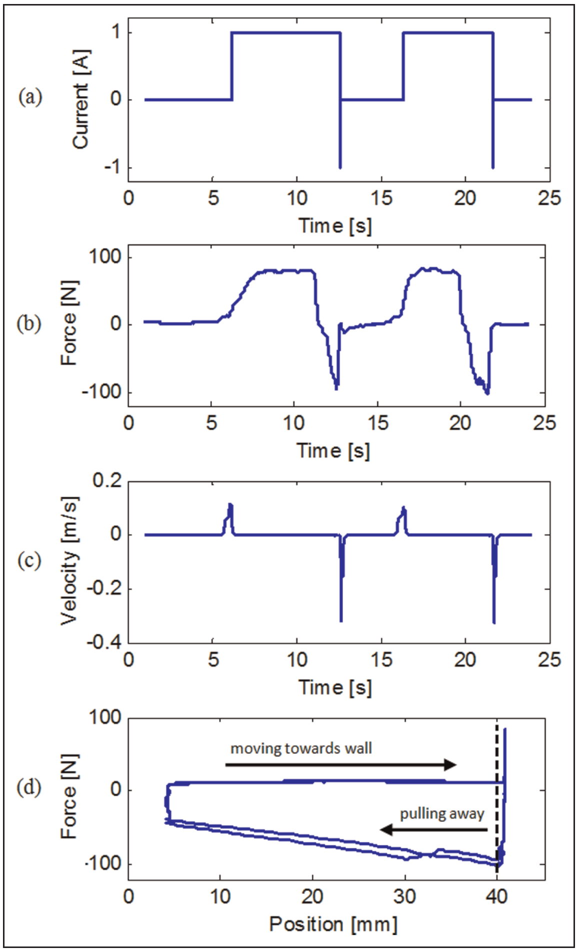

Figure 11. Simulation of collision with a virtual wall located at position 40 mm without using the force sensor: (a) Input current, (b) force, and (c) velocity as a function of time and (d) force exerted by the end-effector with respect to position. The handle is first pulled away from position of the wall through approximately 35 mm. Then, it is pushed toward the virtual wall for collision simulation.

The values of the parameters in this model can be modified to simulate various virtual environments with different frictional properties. In order to illustrate the response of our actuator in simulating such an environment, we consider a sample case here with the velocity-deadband (Δv) at 3 mm/s, the static friction force (F_{static}) at 50 N, and the dynamic friction force ($F_{dynamic}$) at 40 N. Figure 15 presents results of the Coulomb friction modeled by the linear MR brake.

Transient response

In this experiment, the goal was to determine the transient response characteristics and the time constant of the brake. A 25.4 mm/s step input was applied on the brake using the CNC. We also wanted to explore the effect of input current on the response. The experiment was repeated for current levels of 0.4, 0.6, 0.8, and 1 A. Shortly after the rod started to move, we engaged the brake at these current levels and captured the responses (Figure 16). The force output resembles a typical first-order system response. The time it takes the braking force to reach 63.2% of its final value took about 120 ms, which is the time constant of our MR brake. This behavior remained the same even when different current levels were used.

Mixed input and cyclical response

Figure 17 shows the results of following mixed input. In this experiment, the rod of the MR brake was given a constant speed profile for motion, while a mixed input profile for force command (current) was sent to the control system. A trapezoidal input followed by a step and sinusoidal inputs were tested. Due to the hysteresis, the force did not turn off completely, but the brake was

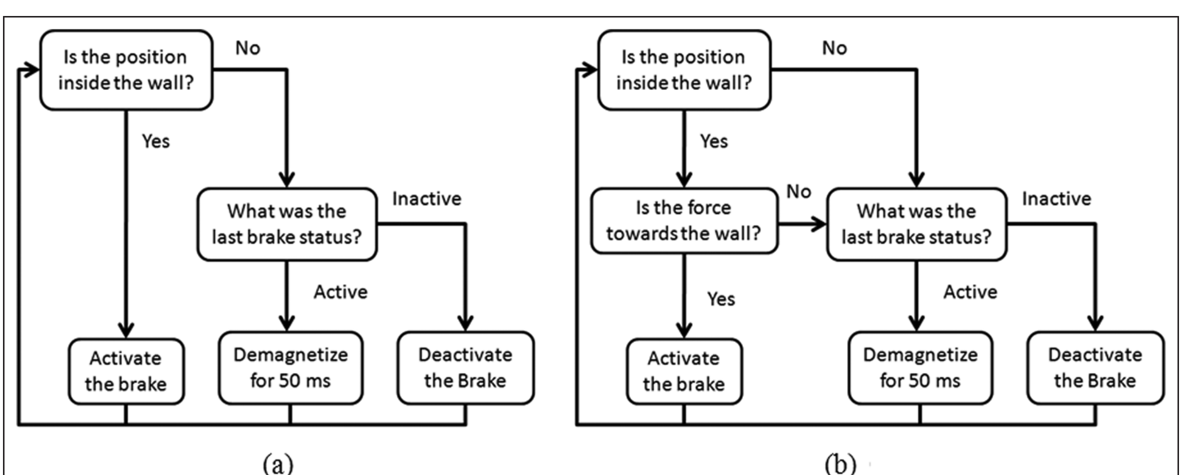

Figure 12. Flow charts for the control strategy followed in the wall collision experiments: (a) control strategy without force sensor and (b) control strategy with force sensor.

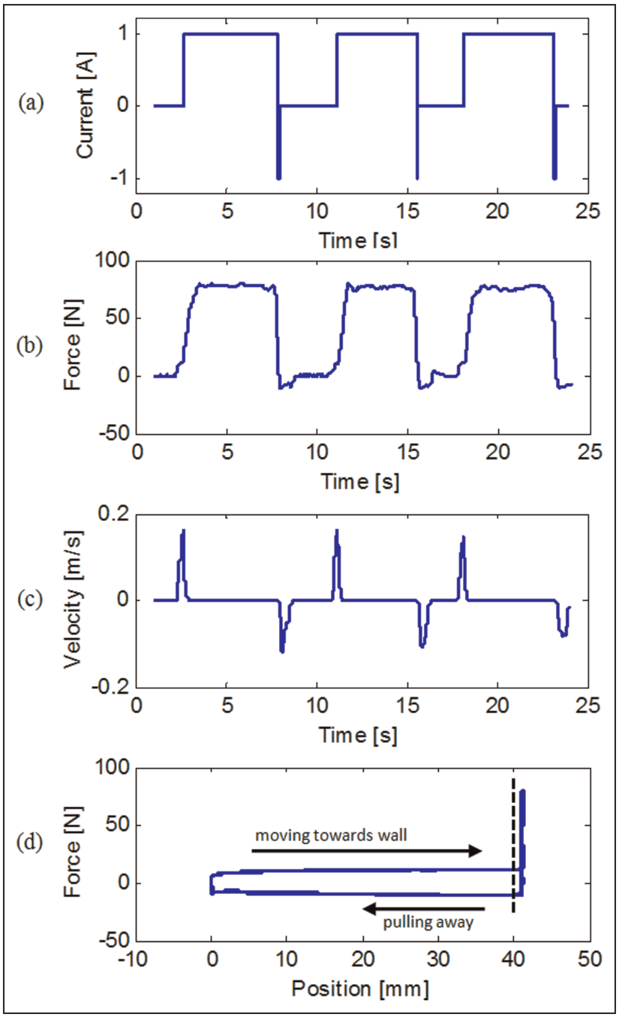

Figure 13. Simulation of collision with a virtual wall located at position 40 mm with the force sensor used in the control system: (a) input current, (b) force, and (c) velocity as a function of time and (d) force exerted by the end-effector with respect to position. The handle is first pulled away from position of the wall through approximately 35 mm. Then, it is pushed toward the virtual wall for collision simulation.

able to follow the input consistently. The maximum force error was about 14%.

Figure 18 shows the results of cyclical push–pull experiment. The performance of the brake has remained consistent, but the effect of the hysteresis can be seen around zero-force level.

Discussion

Figure 9 shows the force output of the MR brake with respect to the current input. The brake shows hysteretic characteristics owing to the magnetization of steel parts. Magnetization in ferromagnetic elements does not vanish even when the magnetic field is removed. The controllability of the MR brake becomes much harder due to this hysteretic behavior of the device. In addition, the off-state force increases since the ferromagnetic elements in the brake continue to exert braking force even when the current input to the brake is turned off.

The total off-state force with the hysteresis is measured as 19.7 N in our experiments after 1 A of coil current is switched on and off. To overcome this extra off-state force, the controller was incorporated an abrupt reverse current pulse when the brake needed to be deactivated. The required reverse current impulse was determined experimentally as 1 A in amplitude and 50 ms in duration (spikes in the current plots in Figures 11 and 13). As a result, the off-state force was reduced to 5.4 N from 19.7 N by collapsing the residual magnetic field.

Simulation of a virtual damper presented in Figure 14 shows this hysteretic behavior even more apparently. Since the device was moved back and forth continuously, there was not enough time for the demagnetization to take place. Due to the effect of this residual magnetism inside the steel parts, the brake showed a highly nonlinear response with hysteresis despite the constant damping coefficient that was used during the simulation. Therefore, the system output two different forces for a corresponding velocity depending on the actuation direction: one for forward and the other for the reverse path of the major hysteretic curve.

Virtual wall simulation with the force sensor showed a sharp increase in the force exerted on the end-effector upon contact with the wall. High rigidity was realized after the contact was prolonged with the wall as shown in Figure 13. The brake abruptly locked the position when the end-effector hits the virtual wall located at 40 mm. After the brake was locked, the force exerted by the brake increased if the end-effector was pushed more into the wall. In this condition, the force values read by the sensor sharply increased to 80 N as shown in Figure 13 at position 40 mm. When the user tried to pull the handle back from the virtual wall, the force exerted by the brake was only the off-state force, which corresponds to about 5.4 N. However, the brake showed a sticky feeling to the user when the force sensor was not included in the control algorithm as seen in Figure 11. The brake was only using the linear encoder to apply force to the user for this case with no clue if the user was trying to pull the handle from the virtual wall or to push against the wall. Once the end-effector collided with the virtual wall, the user had to apply almost as much as the maximum force capacity of the brake to pull the handle away from the virtual wall. This sticky feeling is seen as -100 N force on the wall in the bottom plot of Figure 11.

The performance of the brake for the simulation of Coulomb friction was very good. Being a passive actuator, the MR brake was able to simulate this behavior very easily. Even though the mathematical model of the phenomenon is easy to describe on article, most of the active actuators, capable of adding extra energy to

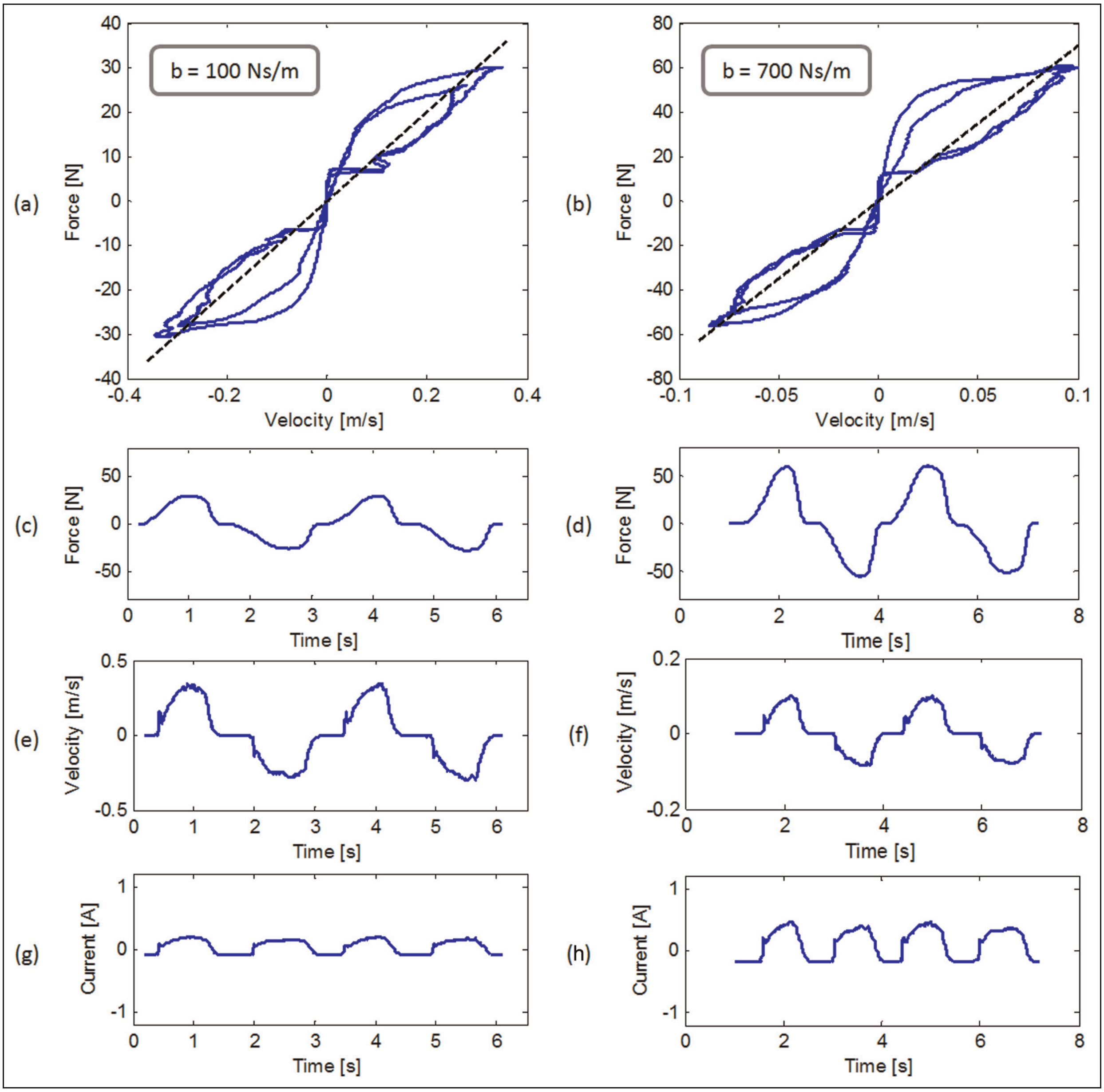

Figure 14. Simulation of a virtual damper using the prototype linear MR brake: (a, b) force as a function of velocity. The desired force is shown with dashed line, where the damping ratio is set to (a) 100 N s/m and (b) 700 N s/m. The force generated by the device is also shown on the same figure: (c, d) force, (e, f), velocity, and (g, h) current as a function of time.
MR: magnetorheological.

the system such as motors, struggle to simulate such discontinuous behavior owing to the stability problems and actuator saturation. Transient characteristic of the system, shown in Figure 16, was similar to that of a first-order system with a time constant of about 0.12 s. The brake successfully produced mixed force profiles (Figure 16). It also performed consistently in cyclical push–pull experiments (Figure 17). In both experiments, the effect of hysteresis could be observed around the zero-force level since the force output could not be completely turned off.

Conclusion

In this research, we developed a compact linear MR brake with infinite stroke and minimal off-state friction force. Employing the serpentine flux path methodology increased the force output of the device. In this approach, the magnetic flux is woven through the MR fluid multiple times activating more of the fluid. The flux guide was shaped by strategically placing magnetically conductive and nonconductive parts in the rod and the casing. Because the geometry became more

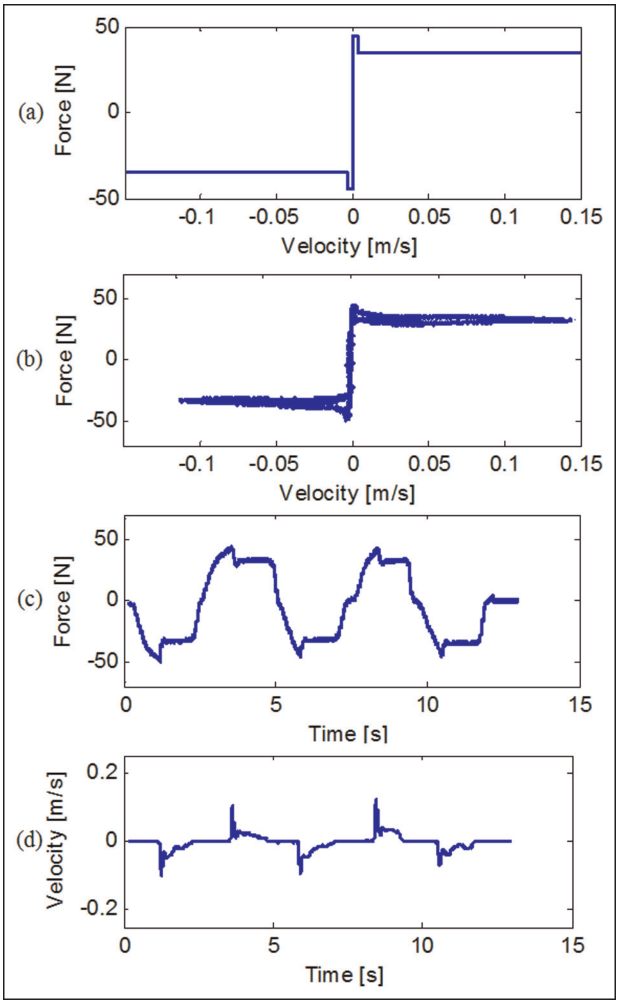

Figure 15. Simulation of Coulomb friction with the prototype linear MR brake: (a) desired input force as a function of velocity. The threshold velocity to model change from static to dynamic friction is 3 mm/s, while the forces for static and dynamic friction are 50 and 40 N, respectively; (b) actual force generated by the prototype device; (c) actual force; and (d) velocity as a function of time.
MR: magnetorheological.

complex in the serpentine design, the manufacturing cost of the brake became larger. The most challenging part was the rod of the brake, which required expensive machining processes to keep high accuracy. Even though the manufacturing was challenging, the resulting device is compact but powerful.

Table 2 compares specifications of our prototype linear MR brake to a number of linear MR brakes in the literature. All other linear MR brakes we could find in the literature were designed using the flow mode of the fluid, which was the main disadvantage resulting in large off-state force. Our approach is a new alternative for the internal design of linear MR brakes. It operates the fluid in the shear mode and minimizes the off-state force. Since we could not find any other linear MR brakes that worked in shear mode, we could only compare our new design with the existing conventional designs. A piston-cylinder device from the literature (Li et al., 2006) that was already optimized by its developers was especially a good representative sample for this comparison. As shown in Table 2, this brake has almost the same size as ours since the cross-sectional areas of both brakes are almost identical, and as the normalized volumes show, the length of the conventional brake is a little longer than ours. Since in both cases, these devices are intended to function as linear dampers, and since we are proposing a completely new internal design alternative for the existing devices, this comparison helped us put our new device in the context of the existing technology.

Another comparison was done by designing a conventional linear MR brake using the same size as our brake. In this design, the rod and piston radii of the conventional linear MR brake were taken to be equal, so that the brake would operate only in shear mode as in our case. We followed the design methodology given by Rosenfield and Wereley (2004). Our brake has an internal space of ~16 mm width. Assuming that the brake is cylindrical and a rod with 8-mm radius is inserted into this space with a single coil wrapped on it following the geometry given in this reference, we ran several iterations to obtain the highest possible braking force.

As pointed out in this study, if the coil depth (w_c) is increased, the size of the coil increases, but this leads to reduced dimensions of the critical magnetic flux paths and reduced size of activated fluid area. Using the coil depth of 5.13 mm from our device, and assuming that the fluid is activated at its maximum shear stress level of 106 kPa as in our design, a conventional linear MR brake will produce an estimated 12.7-N force. In this design, more coil turns than the 250 turns we used would fit on the rod. But this does not improve the force output since it is possible to push the fluid to its maximum activation with just the 250 turns. After that, the fluid activation is saturated.

If the coil depth is reduced down to $w_c = 1$ mm on the same rod, the output force increases since the size of the activated fluid area increases. In this case, the conventional brake produces about 26.6-N force. This design can house about 300 coil turns. As such, it is closer to our 250 turns, but again the fluid activation already saturates passed 250 turns. In comparison, our new design can produce 173-N force in the same physical size. As such, our research makes significant contributions to the state of the art with a new and innovative alternative internal design for linear MR brakes.

Our new design has an infinite stroke. All other similar devices in the literature have finite strokes. Adapting these devices to large-stroke applications is either impossible or can require a drastic increase in the overall actuator size. By using a longer or shorter rod, but

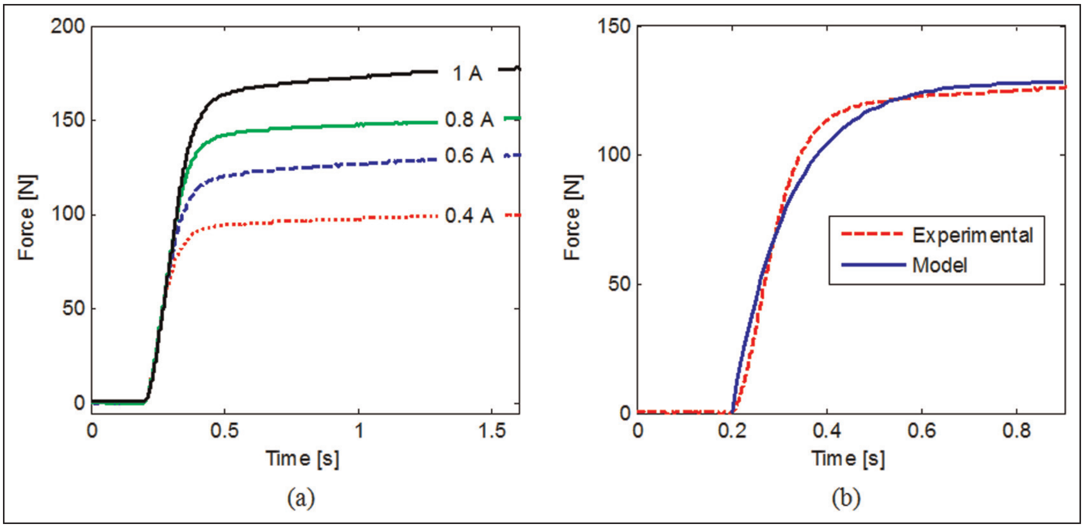

Figure 16. (a) Transient response of the magnetorheological brake. (b) Simulated first-order response overlaid on the experimental data at 0.6 A. The time constant is approximately 120 ms.

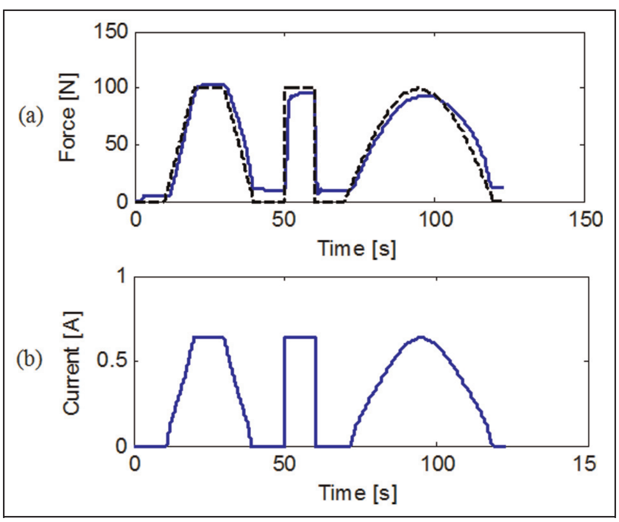

Figure 17. (a) Force response (dashed line), desired force (solid blue) and (b) current input of the magnetorheological brake for a mixed input.

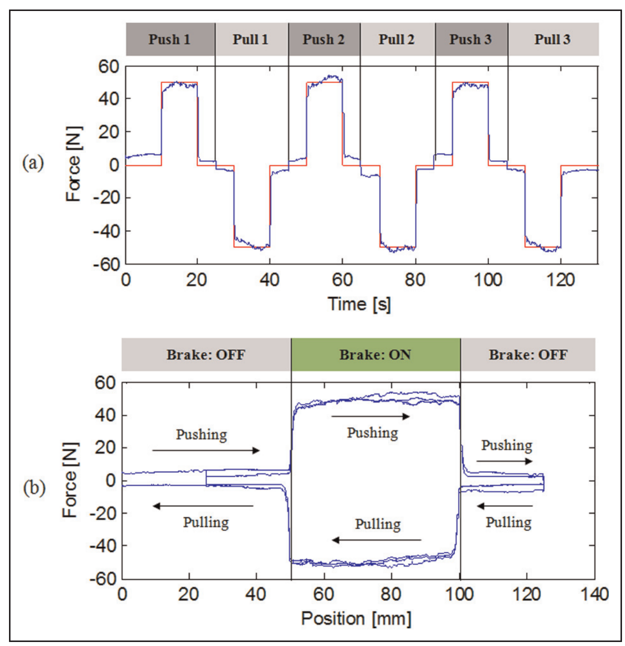

Figure 18. Force response in cyclical push-pull experiment: (a) force versus time; (b) force versus position.

the same actuator casing, our brake can fit into any stroke requirement without requiring size modification on the actuator body. This provides great design flexibility as well as an effective solution against bulky form factors in large-stroke applications. Furthermore, the new brake is quite compact as it is about half the cross-sectional area of a commercially available similar device (RD 8040-1 by Lord Corp.). Finally, when compared with the commercial brake, our prototype has only 3% off-state friction versus 8%–27% in the devices available in the market and the literature. These characteristics improve the potential for the new device to be used in many applications such as haptics, robotics, and automation as a passive actuator.

The linear MR brake was tested as a 1-DOF haptic device. Crisp reaction force was observed at the initial contact in virtual wall collision experiments. During the contact, the brake showed highly rigid response.

Using MR brakes is a viable option in the design of haptic interfaces. Being passive actuators, they are quite safe since they only dissipate energy. Silent operation and relatively fast response are the other main reasons behind their popular use. Despite these advantages, hysteretic response of MR brakes makes their control challenging. Based on this problem, we have recently reported an effective and inexpensive control solution

Table 2. Design specifications of the prototype magnetorheological (MR) brake.

	Our MR brake	RD 8040-1 by Lord Corp.	RD 1005 by Lord Corp.[b]	SD 1000-2 by Lord Corp.[c]	MR brake in the literature[d]	MR brake in the literature[e]	MR brake in the literature[f]
Cross-sectional area of brake (mm^2)	712	1392	1134	1552	707	1678	1963
Volume (mm^3)	79,573	164,256	236,236	158,283	91,892	–	–
Normalized volume[a]	1.0	2.1	3.0	2.0	1.2	–	–
Stroke (mm)	∞	55–74	± 25	60	<107	100	50
Maximum force (N)	173.3	2447	451	2100	942	4000	15000
Maximum off-state force (N)	5.4	667	52	270	94	300	4000
Off-state force/maximum force (%)	**3**	27	12	13	10	8	27
Required supply current for maximum force output (A)	1	1	1.5	1.5	1	10	2.8
Power consumption for maximum force output (W)	15	12	18	–	1.6	60	2.8

[a]For comparison purpose, the volumes of all brakes were normalized using the volume of our MR brake.
[b]Studies of Dominguez et al. (2006), Li et al. (2000), and Xiang et al. (2008).
[c]Study by Li et al. (1998).
[d]Study by Li et al. (2006).
[e]Study by Gavin et al. (2001).
[f]Study by Milecki (2000).

for rotary MR brakes (Erol et al., 2012). Our future work aims to integrate a similar control approach to this new linear brake.

Acknowledgements

The authors would like to thank Mr. Troy Dunmire for his help with the fabrication of the prototype device.

Funding

This research received no specific grant from any funding agency in the public, commercial, or not-for-profit sectors.

References

An J and Kwon DS (2002) Haptic experimentation on a hybrid active/passive force feedback device. In: *Proceedings of the IEEE international conference on robotics and automation*, Washington, DC, 11–15 May 2002.

An J and Kwon DS (2006) Stability and performance of haptic interfaces with active/passive actuators—theory and experiments. *International Journal of Robotics Research* 25: 1121–1136.

An J and Kwon DS (2008) Five-bar linkage haptic device with DC motors and MR brakes. *Journal of Intelligent Material Systems and Structures* 20: 1–12.

Blake J and Gurocak H (2009) Haptic glove with MR-brakes for virtual reality. *IEEE–ASME Transactions on Mechatronics* 14: 606–615.

Dominguez A, Sedaghati R and Stiharu I (2006) A new dynamic hysteresis model for magnetorheological dampers. *Smart Materials and Structures* 15: 1179–1189.

Erol O and Gurocak H (2011) Interactive design optimization of magnetorheological-brake actuators using the Taguchi method. *Smart Materials and Structures* 20: 105027.

Erol O, Gonenc B, Senkal D, et al. (2012) Magnetic induction control with embedded sensor for elimination of hysteresis in magnetorheological brakes. *Journal of Intelligent Material Systems and Structures* 23(4): 427–440.

Gavin H, Hoagg J and Dobossy M (2001) Optimal design of MR dampers. In: *Proceedings of U.S.–Japan workshop on smart structures for improved seismic performance in urban regions*, Seattle, WA, 14 August 2001.

Li C, Furusho J, Morimoto S, et al. (2006) Research and development of the intelligent prosthetic ankle joint with a MR linear brake. In: *Proceedings of the 2006 IEEE international conference on electrorheological fluids and magnetorheological suspensions*, Lake Tahoe, NV, 26–28 June 2006, pp. 534–540. US: IEEE.

Li P, Kamath GM and Wereley NM (1998) Analysis and testing of a linear magnetorheological damper. In: *Proceedings of the 39th AIAA/ASME/ASCE/AHS/ASC structures, structural dynamics, and materials conference and exhibit and AIAA/ASME/AHS adaptive structures forum—Part 4*, Long Beach, CA, 20–23 April 1998.

Li WH, Yao GZ, Chen G, et al. (2000) Testing and steady state modeling of a linear MR damper under sinusoidal loading. *Smart Materials and Structures* 9: 95–102.

Milecki A (2001) Investigation and control of magnetorheological fluid dampers. *International Journal of Machine Tools and Manufacture* 41(3): 379–391.

Nam YJ and Park MK (2007) A hybrid haptic device for wide-ranged force reflection and improved transparency. In: *Proceedings of the international conference on control, automation and systems*, Seoul, Korea, 17–20 October 2007.

Reed M and Book W (2004) Modeling and control of an improved dissipative passive haptic display. In: *Proceedings of the international conference on robotics and automation*, New Orleans, LA, 26 April–1 May 2004.

Rosenfield NC and Wereley NM (2004) Volume-constrained optimization of magnetorheological and electrorheological valves and dampers. *Smart Materials and Structures* 13: 1303–1313.

Senkal D and Gurocak H (2010) Serpentine flux path for high torque MRF brakes in haptics applications. *Mechatronics* 20: 377–383.

Xiang H, Fang Q, Gong Z, et al. (2008) Experimental investigation into magnetorheological damper subjected to impact loads. *Transactions of Tianjin University* 14: 540–544.